Cryobiology 116 (2024) 104943

Contents lists available at ScienceDirect

Cryobiology

journal homepage: www.elsevier.com/locate/cryo

Osmotic injury and cytotoxicity for hMSCs in contact with Me2SO: The effect of cell size distribution

Gabriele Traversari, Antonio Mario Locci, Alessandro Concas, Nicola Lai, Alberto Cincotti *

Dipartimento di Ingegneria Meccanica, Chimica e Dei Materiali, Facoltà di Ingegneria e Architettura, Università Degli Studi di Cagliari, Via Marengo 2, 09123, Cagliari, Italy

ARTICLE INFO

Keywords:
hMSCs
Me2SO
Osmosis
Modelling
Cytotoxicity
Expansion lysis
Cell size distribution

ABSTRACT

The paper discusses the impact of cell size on cytotoxicity and expansion lysis during the osmotic excursions resulting from the contact of hMSCs from UCB with Me2SO. It builds upon the mathematical model recently presented by the authors, which pertains to a population of cells with uniform size. The objective is to enhance the model's relevance by incorporating the more realistic scenario of cell size distribution, utilizing a Population Balance Equations approach. The study compares the capability of the multiple-sized model to the single-sized one to describe system behavior experimentally measured through cytofluorimetry and Coulter counter when, first, suspending hMSCs in hypertonic solutions of Me2SO (at varying osmolality, system temperature, and contact times), and then (at room temperature) pelleting by centrifugation before suspending the cells back to isotonic conditions. Simulations demonstrate that expansion lysis and cytotoxic effect are not affected by cell size for the specific system hMSCs/Me2SO, thus confirming what was found so far by the authors through a single-size model. On the other hand, simulations show that, when varying the adjustable parameters of the model that are expected to change from cell to cell lineages, expansion lysis is sensitive to cell size, while cytotoxicity is not, being mainly influenced by external CPA concentration and contact duration. More specifically, it is found that smaller cells suffer expansion lysis more than larger ones. The findings suggest that different cells from hMSCs may require a multiple-sized model to assess cell damage during osmotic excursions in cryopreservation.

1. Introduction

Human Mesenchymal Stem Cells (hMSCs) represent a highly promising cell type in the fields of regenerative medicine and tissue engineering, owing to their remarkable capacity to differentiate into various tissue types, including cartilage, bones, adipose tissue, muscles, nerves, myocardium, liver, cornea, trachea, and skin [1–4]. These cells can be sourced from diverse origins such as bone marrow, adipose tissue, peripheral blood, placenta, or umbilical cord. Notably, Umbilical Cord Blood (UCB) hMSCs exhibit distinct advantages over other adult sources, such as enhanced growth potential, prolonged cell proliferation, and increased clonality [1,5]. However, the collection and isolation of hMSCs from UCB pose challenges, with instances where no hMSCs are obtained from a single donor. Consequently, the development of a preservation method allowing for long-term storage without compromising cell lineage integrity becomes imperative.

Preserving hMSCs at deep subzero temperatures has been identified as the optimal preservation method [6,7]. Nevertheless, the cooling process for any cells carries the risk of Intracellular and Extracellular Ice Formation (IIF and EIF), posing a potential threat [6–9]. This risk is particularly critical for UCB-derived hMSCs, given the challenges associated with their collection and isolation. In a previous paper [8] the authors emphasized that IIF is more severe for larger cells compared to smaller ones. To mitigate damage during freezing, cryoprotectant agents, such as DiMethylSulfOxide (Me2SO) or glycerol, are employed.

The standard cryopreservation and thawing protocol involve several stages [10]. Harvested cells are centrifuged and immersed in a Cryo-Protectant Agent (CPA) solution, followed by a gradual cooling process to prevent IIF [11]. The frozen cells are then stored in, for example, liquid nitrogen. Upon need, cells are thawed using methods like a water bath, and after thawing, the suspension is centrifuged to concentrate the cells. Subsequently, the removal of the CPA is performed by placing the cells into bathing solution, with potential variations in solution composition during this phase [10]. The primary stages of the cryopreservation protocol are CPA addition, cooling, storage, thawing, and CPA removal.

* Corresponding author.
E-mail address: alberto.cincotti@unica.it (A. Cincotti).

https://doi.org/10.1016/j.cryobiol.2024.104943
Received 29 November 2023; Received in revised form 17 July 2024; Accepted 17 July 2024
Available online 2 August 2024

Throughout these cryopreservation stages, damage may occur due to CPA cytotoxicity or osmotic injuries [12–15]. To avoid costly trial-and-error experiments resulting in the wastage of valuable cells, mathematical models have been developed to enhance the understanding of processes during different stages and optimize subsequent protocols. In Refs. [16,17] the authors introduced a model of a peculiar osmotic behavior based on the 2-parameter model [18]. More specifically, since the 2-parameter model lacks the ability to simulate the behavior of non-perfect osmometers, a model incorporating Surface Area Regulation (SAR) has been proposed [3,19], and, more recently, the authors suggested a novel mathematical model considering the effects of cytotoxicity and expansion lysis based on the SAR model [20].

As outlined by Ref. [20] the consideration of cytotoxic effects and expansion lysis necessitates the categorization of the cell population into viable and nonviable cells. Specifically, the decline in cell count is attributed solely to osmotic injuries resulting from expansion lysis, wherein excessive swelling leads to the rupture of both viable and nonviable cells: in this regard, lysis due to shrinking is re-expansion lysis and not the shrinking itself, as during the shrink-swell dynamics when loading a permeant CPA. Conversely, the decrease in cell viability is exclusively linked to cytotoxicity, a process that progressively transforms viable cells into nonviable ones. To elucidate the dynamics of these phenomena, a chemical reaction engineering approach was employed in Ref. [20]. This involves tracking the kinetics of two chemical reactions occurring during cell osmosis within a closed and perfectly mixed system, whose rates are proportional to CPA intracellular concentration and membrane tension variation with time, correspondingly. The study demonstrated that the simultaneous reduction in cell count and viability can be effectively explained through this approach. The adoption of the SAR model eliminates the need to predefine fixed cell Osmotic Tolerance Limits (OTLs), whereas traditionally cryopreservation literature relies on predetermined OTLs to bypass the mathematical simulation of osmotic injuries.

However, this model assumes uniform cell volumes, i.e., all cells are assumed to be the same size as the average cell, whereas one can easily predict that cell size should play a role: indeed, since osmosis is expected to be faster for smaller cells (due to a larger surface area/volume ratio), as a consequence cytotoxicity (due to its proportionality to intracellular concentration of CPA) and expansion lysis (due to a membrane tension varying proportionally to cell volume in time) are expected to be more harmful for smaller cells as well.

On the other hand, models for simulating the cooling phase in a size-distributed cell population have been presented in the literature by the authors which address IIF (without CPA [8], and with CPA [9]), or investigates the effects of EIF [7]. It was found that larger cells are more prone to develop IIF, but the cell lineage was different (hepatocyte) and the simplistic approach of the 2-parameter model was adopted to describe osmosis. The 2-parameter model was demonstrated not to be capable to describe the peculiar osmotic behavior of hMSCs [3,19].

This work explores the influence of cell size on cytotoxicity and expansion lysis in the context of osmotic excursions resulting from the contact of hMSCs with Me2SO. The research extends the recently presented mathematical model by the authors [20], originally designed for a uniform-sized cell population, to incorporate the more realistic scenario of cell size distribution by means of a Population Balance Equations (PBEs) approach.

A comparison between the capabilities of the multiple-sized model and the single-sized model in describing system behavior as experimentally measured through cytofluorimetry and Coulter counter is first provided (data taken from Ref. [20]). The results reveal that, for the specific hMSCs/Me2SO system, expansion lysis and cytotoxic effects are unaffected by cell size, aligning with previous findings using a single-sized model.

Conversely, when varying model parameters that may change among cell lineages, simulations demonstrate that expansion lysis is sensitive to cell size, whereas cytotoxicity is primarily influenced by external CPA concentration and contact duration. Specifically, smaller cells experience more pronounced expansion lysis than larger ones.

2. Modeling section

This section reports only the PBEs necessary to extend the single-size model for cytotoxicity and expansion lysis recently proposed [20] to the case where a size-distributed cell population is accounted for. The mathematical description of osmosis through the SAR model is identical to papers already published by the authors [3,19,20] and briefly summarized in the appendix section.

When addressing a size-distributed cell population, it is worth focusing into a single size class of the distribution which is representative of any other class as shown in Fig. 1: therefore, in any given size class of cells, both viable and nonviable cells undergo rupture and are transformed to debris thus losing their identity during the swelling process, when membrane tension increases rapidly beyond a critical threshold, following a first-order reaction rate. This phenomenon is illustrated schematically in Fig. 1, depicting the stage of CPA addition (i.e., the contact phase between hMSCs and CPA, before Me2SO is removed by washing in isotonic solutions). During this phase, the well-known shrink-swell dynamics occurs: initially, cell size decreases due to water outflow as CPA accumulates in the cytoplasm, leading to slackening of the cell membrane and a decrease in membrane tension. Subsequently, the cell volume begins to return towards its initial isotonic state due to water inflow while CPA continues to enter the cells. This swelling results in the stretching of the cell membrane, activating mechano-sensitive channels (allowing ion exchange with the suspending solution) and potentially leading to expansion lysis. According to the SAR model, this outflow of intra-cellular ions during the opening of mechano-sensitive channels is responsible of the non-perfect osmometer behavior of hMSCs that do not return to their initial isotonic volume after removing the Me2SO by washing the cells in isotonic solutions. Conversely, Fig. 1 illustrates cytotoxicity induced by Me2SO as the kinetics of a simultaneous reaction: a first-order reaction rate from viable (reactant, green) to nonviable (product, red) cells.

Therefore, according to this picture in any given size class (υ, volume of cells) the cell population is divided into two subpopulations, that is, viable (V) and nonviable (NV) cells, as expressed by the following equation:

$$n_{TOT}(\upsilon, t) = n_V(\upsilon, t) + n_{NV}(\upsilon, t) \tag{1}$$

where $n_i(\upsilon, t) \cdot d\upsilon$ with $i = TOT, V, NV$ represents the number of cells in any subpopulation belonging to a specific size class, i.e. the one with a cell volume between υ and $(\upsilon + d\upsilon)$. As such, $n_i(\upsilon, t)$ is the number of cells with volume υ per unit cell volume, i.e. it is a number density distribution [21,22].

Apart from the osmotic phenomenon that shifts a size class of cells to a contiguous one (from a volume υ to a neighboring one), the two subpopulations of viable and nonviable cells (V and NV) undergo temporal variations following the reaction scheme depicted in Fig. 1. When a sufficient intracellular concentration of the toxic and permeant Me2SO is attained during osmotic excursions, viable cells progressively transform into nonviable ones over time, following the reaction kinetics of the cytotoxic effect. This transformation is responsible for the observed reduction in cell viability, as measured experimentally by flow cytometry. Consequently, the number of viable and nonviable cells is expressed as a function of time (t) in Equation (1), with viable cells acting as the reactant, gradually converting into nonviable cells, representing the reaction product. This reaction can occur during the contact phase (i.e., shrink-swell dynamics during CPA addition) as well as in subsequent stages when the cells are initially pelleted by centrifugation and later suspended back to isotonic conditions (i.e., swell-shrink dynamics during CPA removal), provided that enough Me2SO remains inside the cells.

Notably, this transformation of a cell sub-population into another

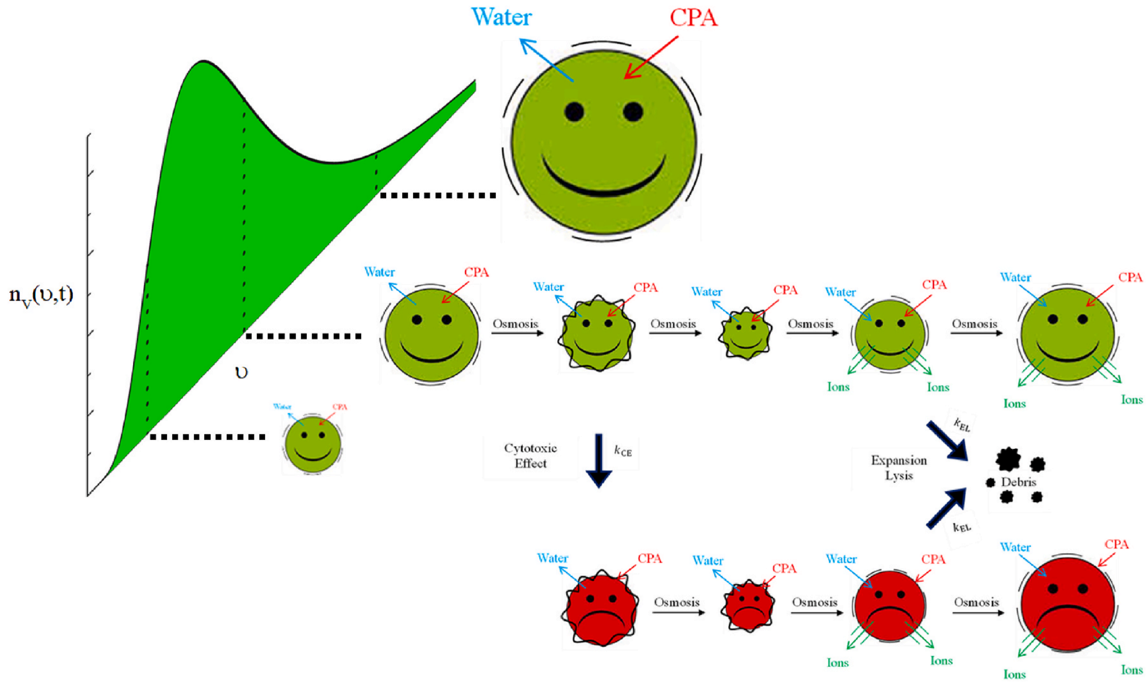

Fig. 1. Schematic representation of cell system response to the addition stage of a toxic CPA like Me2SO, when the shrink-swell dynamics occurs according to the SAR model. In any single size class of the cell size distribution, cells are divided between viable (green) and non-viable (red) cells: viable cells transform into non-viable ones following the reaction kinetics of cytotoxicity when a sufficient amount of intracellular CPA is accumulated; both sub-populations decrease in number due to osmotic injury following the reaction kinetics of expansion lysis, i.e. transforming into lost, undetected cells like debris, when membrane is stretched too rapidly during swelling. Adapted from [23].

does not account for the temporal dependence of the total number of cells, n_{TOT}, presented in Equation (1), which is influenced by the reaction representing expansion lysis shown in Fig. 1 as well. According to this scheme, both viable and nonviable cells act as consumed reactants in the reaction representing osmotic injury, assuming that both sub-populations of cells share the same osmotic response, as illustrated in Fig. 1 for both green and red cells. This assumption holds true under the relatively low Me2SO concentrations employed in the experimental runs considered in this study, where only a decrease in membrane thickness is expected without any leakage effect, as indicated by Ref. [12]. This simplification of the model is applicable during both the contact phase and the subsequent removal phase when the cells are re-suspended back to isotonic conditions. In instances of excessive swelling, expansion lysis transforms viable and nonviable cells into undetectable, lost cells (debris), effectively mirroring the decrease in cell count observed experimentally by the Coulter counter.

Based on this picture, the following 1-D PBEs i.e. the number balances in a closed reacting system for any given size-class of cells may be written along with the corresponding initial (ICs) and boundary conditions (BCs) for viable cells

$$\frac{\partial n_V(\upsilon,t)}{\partial t} = -\frac{\partial[G_\upsilon(\upsilon,t)\cdot n_V(\upsilon,t)]}{\partial \upsilon} - [k_{CE}(\upsilon,t)+k_{EL}(\upsilon,t)]\, n_V(\upsilon,t) \tag{2}$$

$$\text{I.C. } n_V(\upsilon,0) = n^0_{TOT}(\upsilon)\cdot R^0_V \tag{3}$$

$$\text{B.C. } n_V(0,t) = 0 \text{ and } n_V(\infty,t) = 0 \tag{4}$$

as well as for nonviable cells

$$\frac{\partial n_{NV}(\upsilon,t)}{\partial t} = -\frac{\partial[G_\upsilon(\upsilon,t)\cdot n_{NV}(\upsilon,t)]}{\partial \upsilon} + k_{CE}(\upsilon,t)\, n_V(\upsilon,t) - k_{EL}(\upsilon,t)\, n_{NV}(\upsilon,t) \tag{5}$$

$$\text{I.C. } n_{NV}(\upsilon,0) = n^0_{TOT}(\upsilon)\cdot(1-R^0_V) \tag{6}$$

$$\text{B.C. } n_{NV}(0,t) = 0 \text{ and } n_{NV}(\infty,t) = 0 \tag{7}$$

Here the kinetics of the reaction rates representing the cytotoxic effect and expansion lysis, namely ($k_{CE}\cdot n_V$) and expansion lysis ($k_{EL}\cdot n_i$, where $i = V, NV$) respectively, is assumed to be first-order with respect to the corresponding number of cells acting as reactants, whereas $G_\upsilon(\upsilon,t)$ corresponds to the rate of volume change due to osmosis (i.e. $\frac{d\upsilon}{dt}$) as provided by the SAR model and takes into account the osmotic shift of a size class of cells to a contiguous one (from a volume υ to a neighboring one). $G_\upsilon(\upsilon,t)$ depends only on cell volume assuming that both sub-populations of viable and nonviable cells share the same osmotic response, i.e. the same osmotic parameters. The term with $G_\upsilon(\upsilon,t)$ in the Population Balance Equations (2) and (5) corresponds to the advection term (compressible fluid, i.e. non constant density) of a standard material balance transport equation: when $G_\upsilon(\upsilon,t)$ is negative, the size distribution of the cells move to the left of the cell volume domain, towards smaller volumes, thus describing a shrinking phase; conversely, when $G_\upsilon(\upsilon,t)$ is positive, the size distribution of the cells move to the right, towards larger cell volumes, thus describing a swelling phase. As better detailed in the Appendix section, during osmotic shifts the volume trajectories of different cell size classes never cross each other: in other words, larger cells in the size distribution will always remain the (relatively) larger ones at any given time, as well as smaller cells will always remain the (relatively) smaller ones.

The boundary conditions represented by Eqs. (4) and (7) correspond to the so-called *containment condition* which confines cell distributions within a positive but finite cell volume domain, with no cells at the mathematical boundaries of zero and infinite in the cell volume domain of the PBEs. Whereas the initial conditions in Eqs. (3) and (6) are defined on the basis of the viability ratio $\left(R_V(t) = \frac{N_V(t)}{N_{TOT}(t)}\right)$ experimentally evaluated at $t = 0$ (R^0_V).

The total number of cells of any subpopulations ($N_i(t)$ with $i =$ TOT, V, NV) is obtained by summing-up the contributions from any size-class cell, i.e., by considering the zero-th order moment of the corresponding distribution as it follows:

$$N_i(t) = \int_0^{+\infty} n_i(\upsilon, t) d\upsilon \tag{8}$$

By doing this to Eqs. (2) and (5), due to the containment conditions the following equations are derived:

$$\frac{dN_V(t)}{dt} = -\int_0^{+\infty} [k_{CE}(\upsilon, t) + k_{EL}(\upsilon, t)]\, n_V(\upsilon, t)\, d\upsilon \tag{9}$$

$$\frac{dN_{NV}(t)}{dt} = +\int_0^{+\infty} k_{CE}(\upsilon, t)\, n_V(\upsilon, t)\, d\upsilon - \int_0^{+\infty} k_{EL}(\upsilon, t)\, n_{NV}(\upsilon, t)\, d\upsilon \tag{10}$$

which means that while the total number of nonviable cells are produced by cytotoxicity and consumed by expansion lysis, viable cells are consumed by both reactions. The ICs for Eqs. (9) and (10) are

$$N_V(t = 0) = \int_0^{+\infty} n_V(\upsilon, 0)\, d\upsilon = \int_0^{+\infty} n^0_{TOT}(\upsilon)\cdot R^0_V\, d\upsilon = N^0_{TOT}\cdot R^0_V$$

and

$$N_{NV}(t = 0) = \int_0^{+\infty} n_{NV}(\upsilon, 0)\, d\upsilon = \int_0^{+\infty} n^0_{TOT}(\upsilon)\cdot(1 - R^0_V)\, d\upsilon = N^0_{TOT}\cdot(1 - R^0_V).$$

Clearly, according to Eq. (1) by summing-up Eqs. (9) and (10) the balance on N_{TOT} is obtained:

$$\frac{dN_{TOT}(t)}{dt} = -\int_0^{+\infty} k_{EL}(\upsilon, t)\, \overbrace{(n_V(\upsilon, t) + n_{NV}(\upsilon, t))}^{n_{TOT}(\upsilon,t)}\, d\upsilon \tag{11}$$

confirming that, in the proposed model, only expansion lysis is seen as responsible for the decrease of the total number of cells, whereas in any size-class of cells

$$\frac{\partial n_{TOT}(\upsilon, t)}{\partial t} = -\frac{\partial\left[G_\upsilon(\upsilon, t)\cdot\overbrace{(n_V(\upsilon, t) + n_{NV}(\upsilon, t))}^{n_{TOT}(\upsilon,t)}\right]}{\partial\upsilon} - k_{EL}(\upsilon, t)\,\overbrace{(n_V(\upsilon, t) + n_{NV}(\upsilon, t))}^{n_{TOT}(\upsilon,t)} \tag{12}$$

the number of total cells depends also on osmosis, i.e. on cell volume variation in time $G_\upsilon(\upsilon, t)$.

Needless to say that, in the case of a very narrow cell size distribution (i.e. single size model) Eqs. (9)–(11) collapse to the ones reported in the parent paper [20].

In accordance with [20], the kinetic rate constant for the transformation of viable cells into non-viable cells due to the cytotoxic effect k_{CE} is expressed with a generic power-law dependence on the intracellular CPA concentration, along with the Arrhenius-like temperature dependence [23–25]:

$$k_{CE} = k^{\infty}_{CE} \exp\left(-\frac{E_{a,CE}}{R\,T}\right)\left(M^{INT}_{CPA}\right)^{\alpha} \tag{13}$$

so that k_{CE} is not really constant but actually varies due to the temporal changes in M^{INT}_{CPA} during the osmotic excursions, following the SAR model. Furthermore, temperature also changes among the different experimental runs considered in this work. Besides, since M^{INT}_{CPA} depends on cell volume it varies differently among the different cell-size classes of the PBEs: given that intracellular concentration of CPA varies more rapidly in smaller cells than in larger ones, longer contact times with toxic Me2SO are expected for the former ones due to a quicker addition phase, which eventually should lead to a more harmful cytotoxic effect.

Continuing to extend the single-size model from the parent paper to the case of a population of cells distributed in volume, k_{EL} regarding the probability of the expansion lysis occurrence, is determined as

$$k_{EL} = \gamma\,\frac{d\Delta\sigma}{dt} \tag{14}$$

so that even k_{EL} is not really constant but actually varies due to the temporal changes in membrane tension σ during the osmotic excursions, following the SAR model. More specifically, in any size-class of the cell distribution expansion lysis is pictured as a statistical event where cells may reach a membrane tension greater than σ_{Break} without lysis, but its probability increases so much that it will soon occur shortly after. This behavior is modelled by adopting a probability density function f_{EL} for the expansion lysis event like the following Weibull distribution where the so-called shape factor K_W is introduced.

$$f_{EL} = \frac{K_W\,(\Delta\sigma)^{K_W-1}}{(\Delta\sigma_{Break})^{K_W}}\exp\left[-\left(\frac{\Delta\sigma}{\Delta\sigma_{Break}}\right)^{K_W}\right] \tag{15}$$

with the corresponding transition function

$$\gamma = \frac{K_W\,(\Delta\sigma)^{K_W-1}}{(\Delta\sigma_{Break})^{K_W}} \tag{16}$$

while the rate of membrane tension variation $\frac{d\Delta\sigma}{dt}$ is calculated from the SAR model.

Since Δσ depends on cell volume, it varies differently among the different cell-size classes of the PBEs: given that membrane tension varies more rapidly in smaller cells than in larger ones, a more harmful expansion lysis is expected for the smaller cells.

The Eqs. reported above coupled with the SAR model represent the PBEs for the size distributed cell population involving two independent variables, cell volume υ and time t. The system of PDEs is solved numerically with the method of lines, i.e. by discretizing only the domain of cell volume υ, in order to obtain a system of ODEs in time which is integrated through a standard marching procedure as an initial value problem. The numerical algorithm used is identical to that detailed in our previously published works [7–9]. The number of discretization intervals was increased until no differences between the results were visible: the final number of intervals used was 5000.

3. Results and discussion

The values of the model parameters used in this work to describe the cytotoxic effect and expansion lysis for hMSCs in contact with Me2SO are reported in Table 1. They are taken from literature [20] and were obtained by fitting the single-cell model to experimental data measured through cytofluorimetry and Coulter counter, when, first, suspending hMSCs in hypertonic solutions of Me2SO (at varying osmolality, system temperature, and contact times), and then (at room temperature) pelleting by centrifugation, before suspending the cells back to isotonic conditions. In the simulations performed in this work, the initial cell-size distribution $n^0_{TOT}(\upsilon)$ and the corresponding viability ratio R^0_V appearing in Eqs. (3) and (6) are taken from Ref. [20] as well.

In Figs. 2–3 the comparisons between data and model results are shown. In Fig. 2 the decrease of cell count (normalised with the corresponding initial value) measured by the Coulter counter at the end of the removal phase is reported as a function of the vol% of Me2SO used during the contact phase, for every experimental run considered.

Table 1
Parameter values for cytotoxic effect and expansion lysis [20].

Parameter	Value	Unit
k^0_{CE}	61.785	$[L^{\alpha}\ s^{-1}\ mOsm^{-\alpha}]$
$E_{a,CE}$	92816.592	$[J\ mol^{-1}]$
α	3.0822	[-]
K_W	2.5456	[-]
σ_{Break}	10985.156	[Pa]

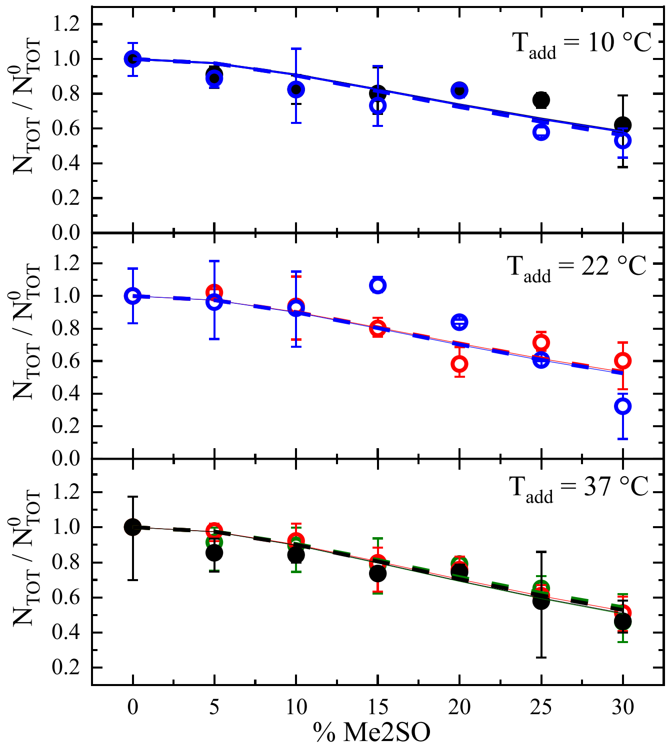

Fig. 2. Normalised cell count measured by Coulter counter at the end of the removal phase as a function of vol% of Me2SO used during the contact phase: varying the temperature during the contact phase 10 °C; 22 °C; 37 °C, and contact times 5 min, 30 min, 60 min, 120 min. Symbol represents measured data, thin solid line represents the solution obtained by the single-size model, dashed line represents the solution obtained by the multiple-size model (cfr. Eq. (11)). Adapted from [23].

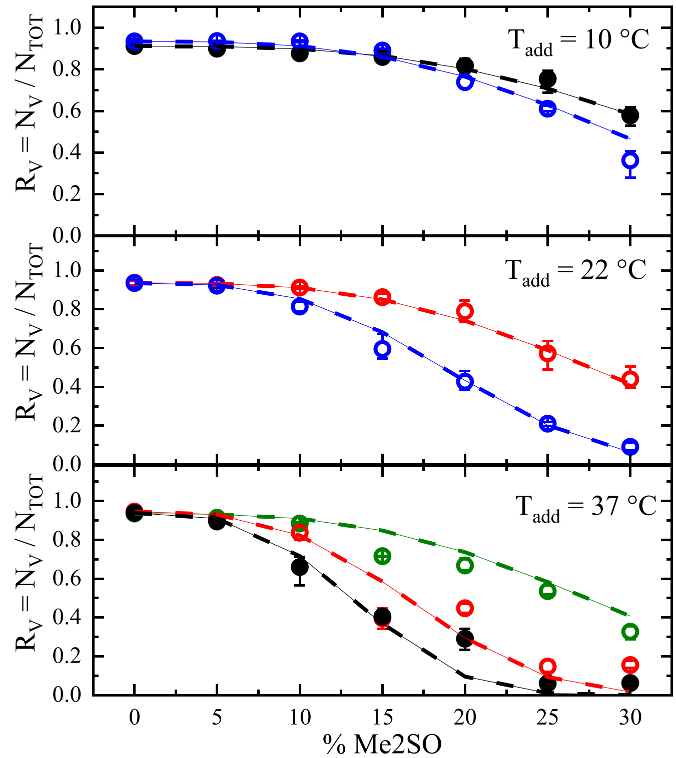

Fig. 3. Viability ratio measured by flow-cytometer at the end of the removal phase as a function of vol% of Me2SO used during the contact phase: varying the temperature during the contact phase 10 °C; 22 °C; 37 °C, and contact times 5 min, 30 min, 60 min, 120 min. Symbol represents measured data, thin solid line represents the solution obtained by the single-size model, dashed line represents the solution obtained by the multiple-size model (cfr. Eqs. (10) and (11)). Adapted from [23].

Analogously, in Fig. 3 the decrease of viability ratio measured by the flow-cytometer at the end of the removal phase is shown as a function of vol% of Me2SO used during the contact phase. For the sake of comparison, separated data are shown for the three temperature levels used during the contact phase, while the varying contact time is accounted for by using different colors, that is, 5, 30, 60, and 120 min, for data (closed circle) as well as theoretical results: for the latter ones, solid lines represent the single-size model while the dashed lines correspond to the model accounting for the cell size distribution.

It is apparent that the multiple-size model unmistakably coincides entirely with the single-size model, demonstrating their equal effectiveness in describing experimental data.

For this reason, only the simulations provided by the model of the cell size distribution are reported in Fig. 4 where the focus is on a single experimental run. Here the selected case taken as representative combines the shortest addition phase (5 min) with the highest temperature (37 °C) and Me2SO concentration (30 %) among the operating conditions investigated in Figs. 2–3. As clearly shown in Fig. 4a, viable and nonviable cells share the same osmotic excursions in terms of mean cell volume (calculated as 1-st moment/zero-th moment of the cell size distribution, $\frac{\int_0^{+\infty} \upsilon \cdot n_i(\upsilon, t) d\upsilon}{\int_0^{+\infty} n_i(\upsilon, t) d\upsilon}$ with i = TOT, V, NV), i.e., shrink-swell dynamics during CPA addition, followed by swell-shrink dynamics during removal. Noteworthy, according to the SAR model hMSCs do not act as perfect osmometers and cell volume does not go back to its initial, isotonic value due to leakage of intracellular ions during swelling, when membrane stretching leads to the opening of mechano-sensitive

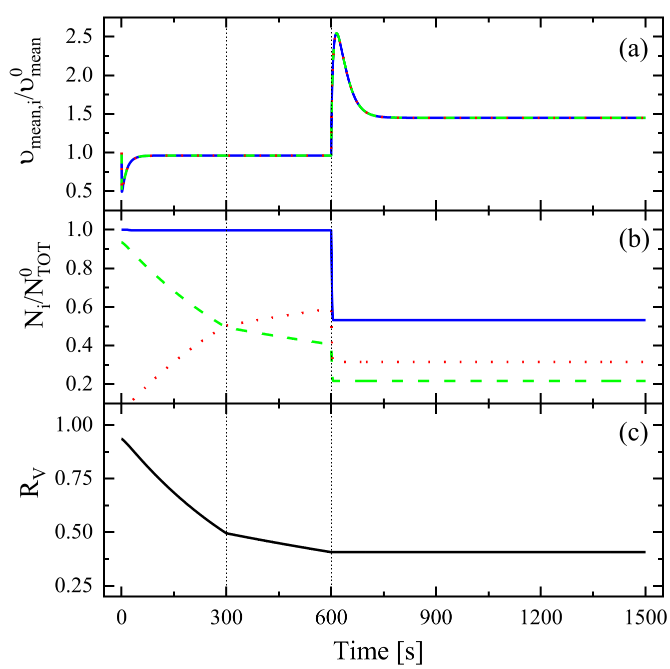

Fig. 4. Temporal profiles from the multiple-size cell model of normalised mean cell volume (a), cell count (b), and viability ratio (c) for the case of 5 min, 37 °C, and 30 % for duration, temperature, and Me2SO concentration in the addition phase (solid blue for total cells, dashed green for viable cells, dotted red for nonviable cells).

channels. As a whole, these results corroborate the conclusion that expansion lysis and cytotoxicity impact the hMSCs regardless of their size, and that changes in mean cell volume are primarily due to cell osmotic response.

Besides, the temporal profiles of cell counts reported in Fig. 4b point out that, during the addition ($t \leq 300$ s) and centrifugation ($300\ \text{s} < t < 600\ \text{s}$) phases, total cell number remains constant even though viable cells are gradually transforming into non-viable ones, so that the viability ratio decreases with time as reported in Fig. 4c; this continues up to a certain point in time when, with the beginning of the removal phase ($t \geq 600$ s), an abrupt decrease of total cell number due to expansion lysis occurs, and viability ratio stops decreasing.

The corresponding cell size distributions for total, viable and nonviable cells at the beginning of the addition phase as well as at the end of the removal phase are reported in Fig. 5. The distributions are reported as normalised to the corresponding cell count (cfr. Eq. (8)): this way the area under the curve is always equal to 1 making it easier to compare between different instants in order to identify any effects of the size distribution. As clearly shown in Fig. 5, viable and nonviable cells behave the same: a shift toward larger volumes in comparison to the initial isotonic conditions due to the non-perfect osmometer behavior, even though Fig. 4 shows that initially the count of viable cells decreases in favor to a growing number of nonviable cells due to cytotoxicity during CPA addition, and lately both decreases abruptly with the beginning of CPA removal due to expansion lysis. To demonstrate this, Fig. 6 shows the same simulations reported in Fig. 5 but neglecting ion-leakage: now no shift to large volumes occurs. Removing ion leakage in Fig. 6 eliminates the rightward shift in distribution observed in Fig. 5, while the reduction in count and viability (not shown for brevity) remains practically unchanged (about 50 % and 40 %, respectively). Evidently, with the parameters in Table 1, both cytotoxicity and expansion lysis do not discriminate between large and small cells and affect the different classes in the same manner.

Therefore, a single-size analysis proves to be more than adequate in capturing cytotoxicity and expansion lysis phenomena in the interaction between hMSCs and Me2SO. This validation underscores the robustness of the findings published by the authors thus far, utilizing a single-size model for the examined system.

However, things may change for different cell lineages, i.e., when using different model parameters for the cytotoxic effect and expansion lysis. Indeed, the values of the model parameters reported in Table 1 are strictly related to expansion lysis and cytotoxic effect for hMSCs in contact with Me2SO and are expected to vary when focusing on another

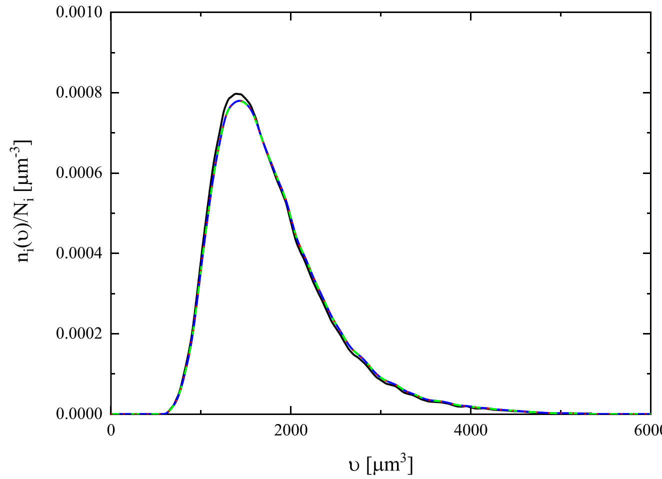

Fig. 6. Normalised cell size distributions for the same case shown in Fig. 5 but neglecting ions leakage: start of the addition phase (solid black line), end of the removal phase after 1500 s
(solid blue for total cells, dashed green for viable cells, dotted red for nonviable cells).

cell-line and/or a different CPA: for example, it is likely that for a different cell line in contact with the same Me2SO, a different value should be used for α (the power law exponent in Eq. (13) adopted for the reaction rate representing the cytotoxic effect). For this reason in the following the value of the parameters appearing in Table 1 is varied when simulating with the model accounting for the cell size distribution. However, before doing this, to highlight the effect of cell size on cytotoxicity and expansion lysis, these simulations are performed by neglecting the ion-leakage during swelling, i.e., setting equal to zero the transmembrane permeability of ions, in order to avoid the masking effect of a non-perfect osmosis as demonstrated above by comparing Figs. 5 and 6. This way, at the end of the removal phase when isotonic conditions are restored, cell volume is expected to return to its initial, isotonic value (i.e. a perfect osmometer behavior); if this does not occur, a non-negligible effect of cell size on cytotoxicity and/or expansion lysis becomes markedly apparent.

Fig. 7 shows model results analogous to those shown in Fig. 6, i.e., referring to the same operating conditions but adopting a value for parameter α appearing in Eq. (13) equal to 3.2 (slightly larger than the one reported in Table 1 for hMSCs with Me2SO), and completely

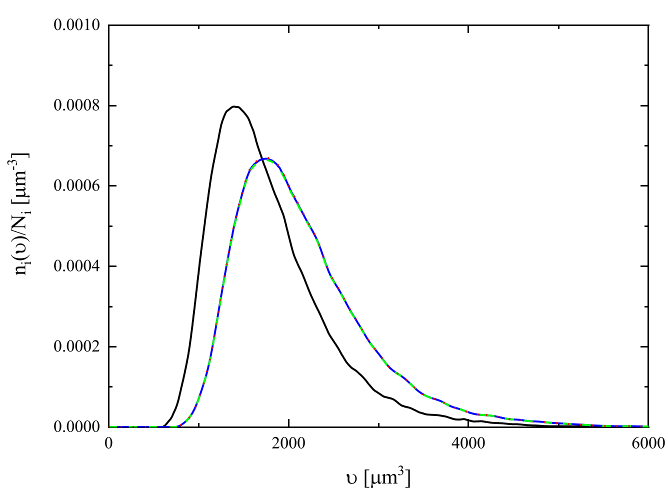

Fig. 5. Normalised cell size distributions for the same case shown in Fig. 4: start of the addition phase (solid black line), end of the removal phase after 1500 s
(solid blue for total cells, dashed green for viable cells, dotted red for nonviable cells).

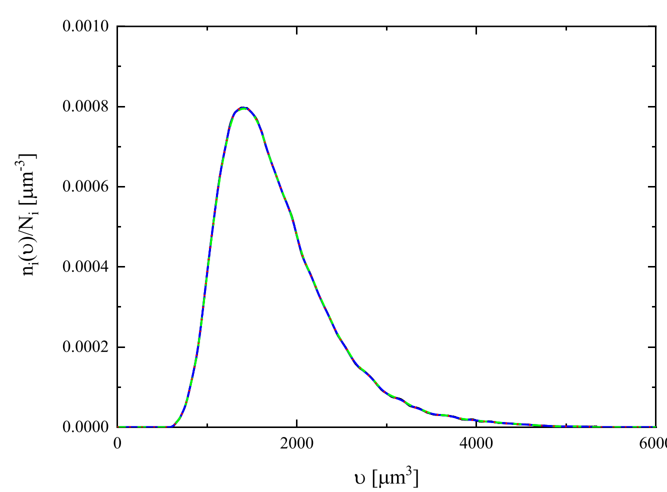

Fig. 7. Normalised cell size distributions for the same case in Fig. 5, but with $\alpha = 3.2$ and neglecting ions leakage and expansion lysis: start of the addition phase (solid black line), end of the removal phase after 1500 s
(solid blue for total cells, dashed green for viable cells, dotted red for nonviable cells).

neglecting expansion lysis by setting $k_{EL} = 0$. This way, only the effect of cell size distribution on cytotoxicity should be accounted for. This specific value of α is selected to enhance cytotoxicity, but with a deliberate limitation to avoid excessive impact, aiming to ensure an observable presence of viable cells by the conclusion of the simulation (resulting in a final viability ratio of approximately 16 %). Further escalation of α would lead to the near complete demise of all cells.

These results suggest that there are no apparent differences in the cytotoxic effect on small and large cells, even with an increase in α. Most of the time, cells of all sizes are similarly affected by cytotoxicity, as the intracellular concentration of CPA remains largely consistent across them. Even if at the beginning of the addition phase the rate of increasing intracellular CPA osmolarity is slightly different between small and large cells, this difference is negligible or balanced by the opposite disproportion at the beginning of the removal phase. This result is obviously the consequence of a significantly higher rate of osmosis than the reaction rate representing cytotoxicity. Even if not shown for the sake of brevity, the total number of cells does not vary in this simulation of course, since expansion lysis is neglected, and cytotoxicity can only transform viable into nonviable cells.

Finally, the last simulation shown in Fig. 8 is performed with the aim to highlight the effect of cell size distribution on expansion lysis. Therefore, the same operating conditions used for Fig. 7 are here used as well, but with a remarkable increase of K_W to 20, and a slight decrease of σ_{Break} to 9000 Pa with respect to the values reported in Table 1 for hMSCs. This choice is easily justified by considering that, as already noted in the parent paper [20], while in Table 1 the value assigned to σ_{Break} is reasonable and comparable with similar ones previously published in the literature, much greater uncertainty is associated with the value assigned to K_W: this latter one is then expected to vary more from cell-to-cell lineage.

Since cytotoxicity is not affected by cell size distribution as demonstrated in Fig. 7, the original value equal to 3.0822 is kept for α in the simulation shown in Fig. 8, where cells acting as perfect osmometers (i.e. ion-leakage neglected) are assumed as well. It is apparent that the final distribution is now shifted to the right, indicating that expansion lysis primarily targets the smaller cells while preserving the larger ones. Both viable and non-viable cells are equally destroyed provided that they reach a sufficiently small size during osmotic excursions, resulting in a subsequent decrease in cell count.

To demonstrate that in this simulation the single- and multiple-size cell models do not match but predict a different behavior, the corresponding temporal profiles of normalised mean cell volume from the multiple-as well as the single-size cell models, cell count, and viability ratio are reported in Fig. 9. Here the same experimental run of Fig. 8 is simulated, i.e. with identical operating conditions and model parameters, so that, essentially, Fig. 9 corresponds to Fig. 8 in the same way that Fig. 4 corresponds to Fig. 5. As clearly shown in panel (a) of Fig. 9, the osmotic excursions of viable, not viable, and total cells cannot be distinguished within the multiple- or the single-size cell model, given that a key assumption of both models is that viable, not viable, and total cells share the same osmotic response. However, the multiple- and single-size cell models differ only after 600 s, when CPA removal starts, after CPA addition ($t \leq 300$ s) and centrifugation ($300 \text{ s} < t < 600 \text{ s}$) have been completed. This is valid also for panel (b) where the temporal profiles of the number of viable, not viable and total cells are reported, whereas a complete overlapping at any time is shown in panel (c) for the temporal profile of the viability ratio.

On the contrary, in every single panel of Fig. 4 a complete overlapping at any time is obtained between multiple- and single-size cell models (the latter one is not shown only for the sake of clarity). Therefore, by comparing Fig. 9 with Fig. 4 it is apparent that, for the case simulated in Fig. 8 single- and multiple-size cell models do not match but predict a different behavior: in particular, referring to panel (a) of Fig. 9 in the single-size cell model the initial, isotonic cell volume is perfectly restored at the end of the simulation, whereas an ultimate larger cell volume is reached in the multiple-size cell model, even though both neglect ion leakage. This different behavior is due to expansion lysis acting differently between single- and multiple-size cell models: more specifically, in the single-size cell model all cells—whether viable, non-viable, or total—are destroyed by expansion lysis during CPA removal, as shown in panel (b) where the cell numbers all drop to nearly zero. Conversely, in the multiple-size cell model a residual fraction of cells is still available after CPA removal (about 16 % in total), since smaller cells are preferentially destroyed leaving untouched the larger ones. Accordingly, a mean cell volume larger than the initial isotonic one is ultimately reached in panel (a) for the multiple-size cell model.

This result is the direct consequence of the specific choice made for the values of K_W and σ_{Break} on probability density function f_{EL} and the

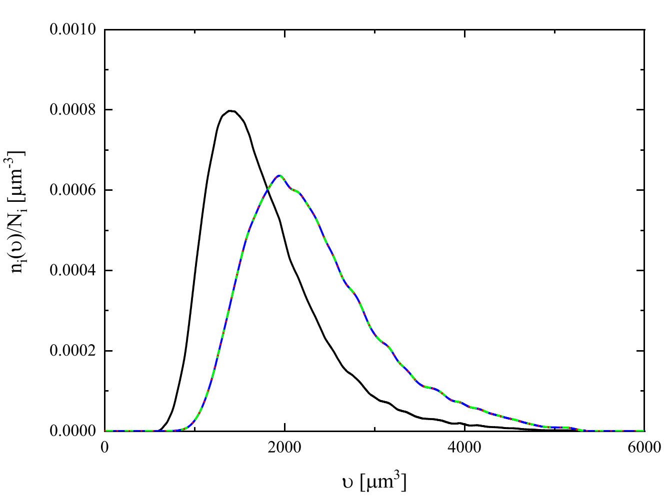

Fig. 8. Normalised cell size distributions of total cells for the same case in Fig. 5, but with $K_W = 20$, $\sigma_{Break} = 9000$ Pa, and neglecting ions leakage: start of the addition phase (solid black line), end of the removal phase after 1500 s (solid blue for total cells, dashed green for viable cells, dotted red for nonviable cells).

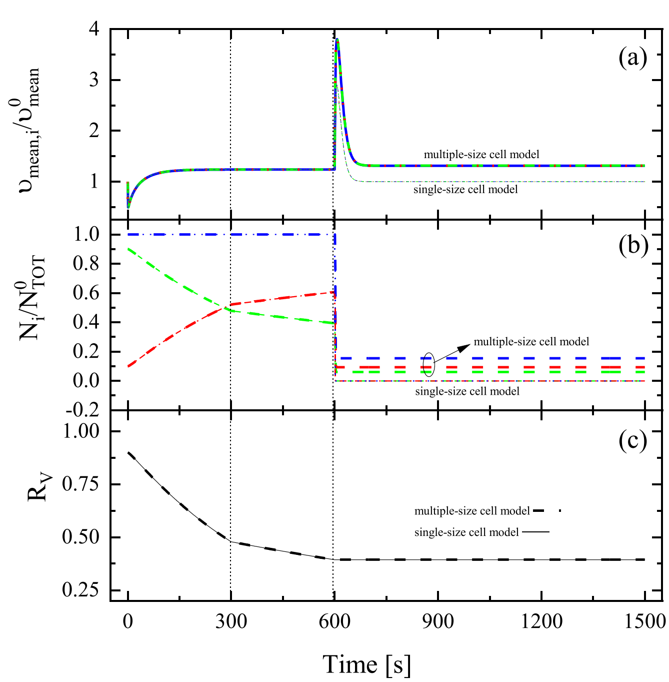

Fig. 9. Temporal profiles from the multiple- and the single-size cell models of normalised mean cell volume (a), cell count (b), and viability ratio (c) for the same case in Fig. 8
(solid blue for total cells, dashed green for viable cells, dotted red for nonviable cells).

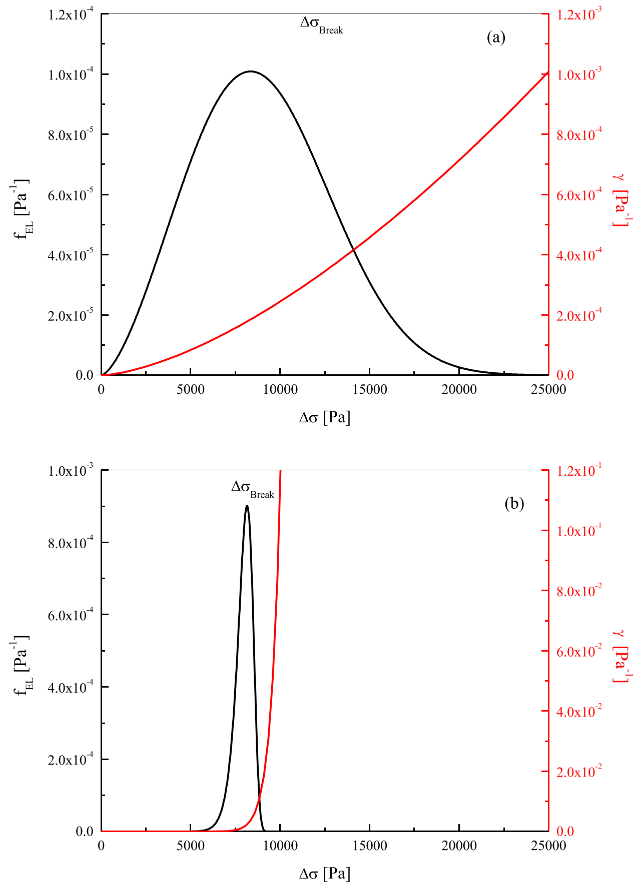

Fig. 10. Comparison of f_{EL} and γ functions for hMSCs (a) and another cell lineage (b) simulated in Figs. 8–9.

corresponding transition function γ, which are plotted in Fig. 10b in comparison with the ones related to the original values of model parameters taken from Table 1 which are drawn in Fig. 10a. As σ_{Break} decreases, the mode of probability density function f_{EL} for expansion lysis occurrence shifts towards smaller $\Delta\sigma$ values. On the other hand, as K_W increases, this distribution narrows around $\Delta\sigma_{Break}$, and the corresponding transition function γ rises sharply to high values (three orders of magnitude higher). This way, a smaller portion of cells is affected by expansion lysis (only that one whose $\Delta\sigma$ reaches sufficient values, i.e., the smaller cells), leaving untouched the other part. On the other hand, if the original σ_{Break} of hMSCs was kept, almost none of the cells would reach such high membrane tension, and no cells would be destroyed by expansion lysis. However, if σ_{Break} decreases too much, all cells eventually burst, and no difference between small and large cells can be seen anymore.

It is worth noting that also the rate of membrane tension variation $(d\Delta\sigma/dt)$ has a significant impact on the expansion lysis rate k_{EL} expressed in Eq. (14). Indeed, according to the SAR model $d\Delta\sigma/dt$ varies proportionally to the rate of cell volume change (dv/dt). Therefore, it is precisely due to a larger surface-to-volume ratio that smaller cells can alter their relative volume more rapidly than larger ones, thus developing more quickly a higher membrane tension, which inevitably leads to their lysis.

The misalignment between single- and multiple-size cell models shown in Fig. 9 may increase or decrease, depending on the specific choice for the values of expansion lysis model parameters as well as operating conditions for the experimental protocol.

4. Conclusions

This study extends the analysis of cytotoxicity and expansion lysis recently introduced [20] from a single-size model to a multi-size model. This extension involves integrating the chemical reaction engineering approach utilized to describe cytotoxicity and expansion lysis rates for both viable and nonviable cells (coupled with the description of osmosis provided by the SAR model) into the Population Balance Equations (PBEs).

Upon comparing the outcomes of the distributed cell size model with the single-sized model, a precise alignment is observed. This alignment suggests that the assumptions previously made by the authors in the parent paper, concerning hMSCs in contact with Me2SO using a single-sized model, remain valid. Consequently, a single-sized model can be efficiently employed, resulting in significant computational savings. Nevertheless, simulations involving variations in parameter values within reasonable ranges indicate that different cell lineages may necessitate the more accurate multi-sized model for evaluating cell damage during osmotic cycles.

Specifically, numerical simulations reveal that only expansion lysis appears to be sensitive to cell size, whereas cytotoxicity is primarily influenced by the external CPA concentration and the duration of the contact phase between cells and toxic Me2SO. Smaller cells exhibit greater susceptibility to damage from excessive osmotic excursions compared to larger cells.

It is noteworthy that during the cooling stage, previous demonstrations have established that larger cells experience more IFF than smaller ones. This implies that the likelihood of cell survival at the conclusion of cryopreservation is higher for a limited subset of cells within a specific volume range: larger cells are prone to suffer IIF, while smaller ones are affected by expansion lysis. Maximizing the survival of the central portion of the initial cell size distribution subjected to a complete cryopreservation protocol could be achieved through numerical simulations.

CRediT authorship contribution statement

Gabriele Traversari: Writing – review & editing, Writing – original draft, Formal analysis, Data curation. **Antonio Mario Locci:** Writing – review & editing, Writing – original draft, Conceptualization. **Alessandro Concas:** Writing – review & editing, Writing – original draft, Conceptualization. **Nicola Lai:** Writing – review & editing, Writing – original draft, Conceptualization. **Alberto Cincotti:** Writing – review & editing, Writing – original draft, Visualization, Validation, Supervision, Software, Project administration, Methodology, Investigation, Formal analysis, Data curation, Conceptualization.

Acknowledgments

This project was funded by the European Union's Horizon 2020 research and innovation program under grant agreement No. 101131087. The funders had no role in the study design, data collection, and analysis, decision to publish, or preparation of the manuscript.

Dr. Jakub Stas is gratefully acknowledged for his help in the numerical solution of the mathematical model

APPENDIX

In the SAR model, cellular osmosis is integrated with considerations of cellular mechanics and the regulation of cell membrane surface area. This model enhances the conventional 2-parameter model commonly utilized in cryopreservation studies by permitting the contingent transmembrane permeation of ions/salt. This permeation occurs through the transient opening of mechanosensitive (MS) channels in response to membrane stretching. Consequently, cells have the capacity to attain an equilibrium volume distinct from their initial volume when contacted to impermeant or permeant solutes, such as sucrose or a cryoprotectant agent like Me2SO, respectively. In contrast, the classical 2-parameter model and Kedem-Katchalsky formalism dictate that cells consistently revert to their isotonic volume, exhibiting perfect osmometer behavior.

For any single size class of the cell distribution, the equations of the SAR model are compiled in Tables A1-A2, with Ordinary Differential Equations (ODEs) separated from auxiliary Algebraic Equations (AEs). A comprehensive discussion regarding these equations, along with its development, is available in existing literature [19], thus obviating the need for redundant exposition within this work. Even the symbolism is to be taken from the literature. Herein, only a succinct overview is provided.

In essence, the SAR model conceptualizes a cell under isotonic conditions akin to an expandable balloon, with its surface, denoted as S_{Sph}, initially stretched from a reference value, S_{Ref}, under a resting tension, σ_{R}, symbolizing a state of homeostasis as delineated by the initial condition in Equation A.4. In response to an osmotic gradient $\Delta\mathrm{M}$ (defined in Equations A.11-A.16), the cell undergoes inflation or deflation through the exchange of water, cryoprotective agents (CPA), and ions with the extracellular compartment, thereby altering its spherical volume, υ and membrane surface area, S_{Sph}, as determined by Equations A.5 and A.9, respectively. Consequently, the ratio $S_{\mathrm{Sph}}/S_{\mathrm{Ref}}$ deviates from its resting value $\left(1+\frac{2\,\sigma_{\mathrm{R}}}{K}\right)$ in proportion to the cell membrane tension, σ, indicative of an elastic response from a mechanical perspective, with K representing the non-dimensional elastic modulus defined in Equation A.8.

This variation yields two notable consequences: firstly, as per the Laplace law (Equation A.6), a counter-gradient of hydrostatic pressure, $\Delta\mathrm{P}$, emerges perpetually opposing the osmotic driving force, $\Delta\mathrm{M}$, in the water exchange rate (note the opposing signs of the two driving forces in Equation A.1). Secondly, mechanosensitive (MS) channels open to facilitate ion exchange (inward or outward, contingent upon their respective gradients) when the membrane is stretched, i.e., when $\sigma > \sigma_{\mathrm{R}}$ or $\left(S_{\mathrm{Sph}}/S_{\mathrm{Ref}}\right) > \left(1+\frac{2\,\sigma_{\mathrm{R}}}{K}\right)$, as elucidated in Equation A.17. However, the deviation of membrane tension from the resting condition is transient owing to membrane relaxation governed by Equation A.4. Eventually, it dissipates through the exchange of surface area with membrane reservoirs, thereby restoring the membrane tension to its resting value and preserving cellular homeostasis.

The extension of the SAR model to the case of a cell size distribution implies that, for any single size volume class the $\mathrm{G}_{\upsilon}(\upsilon,\mathrm{t})=\frac{d\upsilon}{dt}$ appearing in Eqs (2) and (5) is evaluated according to Eq. A.5 as $\mathrm{G}_{\upsilon}(\upsilon,\mathrm{t})=\frac{d\upsilon_{\mathrm{W}}}{dt}+\frac{d\upsilon_{\mathrm{Ions}}}{dt}+\frac{d\upsilon_{\mathrm{CPA}}}{dt}$ by means of Eqs. A.1-A.3. In this context, it is important to emphasize the impossibility that during osmotic shifts cells with different initial volumes (but sharing all the other osmotic parameters like permeabilities of water, CPA and ions namely L_{P}, P_{CPA}, and P_{Ions}, as well as the osmotic inactive fraction ν_{B}) have equal volumes at later time points, i.e. their volume trajectories in time never cross. To demonstrate this, the following Figure A1 reports the volume trajectories of three cells with different initial volumes (i.e. small, medium, and large) during Me2SO loading phase (shrink-swell) and subsequent removal phase (swell-shrink) as simulated by the SAR model for the same operating conditions used in the run shown in Figs. 4–5.

The reason of this behavior is that cell volume variations ($\mathrm{G}_{\upsilon}(\upsilon,\mathrm{t})=\frac{d\upsilon}{dt}$) and its components ($\frac{d\upsilon_{\mathrm{W}}}{dt}$, $\frac{d\upsilon_{\mathrm{Ions}}}{dt}$, $\frac{d\upsilon_{\mathrm{CPA}}}{dt}$) are proportional to cell membrane surface area S_{Sph} (cfr. Eqs. A1-A3). Moreover, this feature is regardless of accounting for a transient or a constant membrane surface area. Therefore, the curves shown in Figure A1 never intersect, and at any given time a unique $\mathrm{G}_{\upsilon}(\upsilon,\mathrm{t})$ may be ascribed to any single class cell volume.

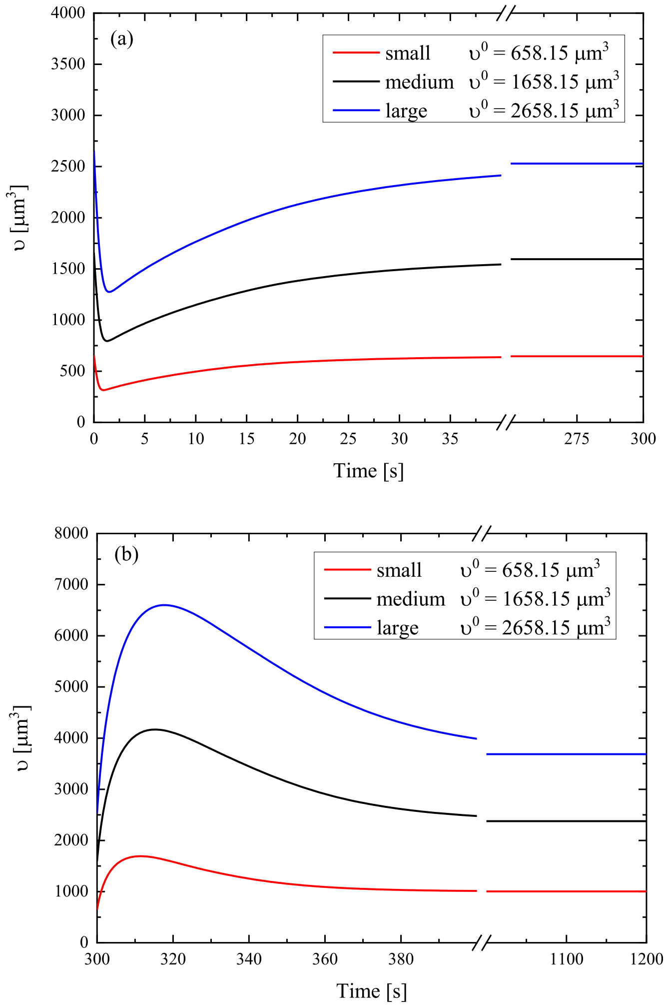

Fig. A1. Cell volume trajectories of three size classes of the cell size distribution starting from different initial volumes (i.e. small, medium, and large) during Me2SO loading phase (a) shrink-swell dynamics and subsequent removal phase (b) swell-shrink dynamics, as simulated by the SAR model for the same operating conditions used in the run shown in Figs. 4–5.

Table A1
ODEs of the SAR model [20].

Equation	Initial Condition	Number
$\frac{d\upsilon_W}{dt} = -L_P S_{Sph}(\Delta P - \Delta\Pi)$	$\upsilon_W(0) = \upsilon_W^0 = \left(\upsilon^0 - \upsilon_{Ions}^0 - \upsilon_B\right)$ @ $t = 0$	(A.1)
$\frac{d\upsilon_{CPA}}{dt} = -\widetilde{\upsilon}_{CPA}\, P_{CPA} S_{Sph} \Delta M_{CPA}$	$\upsilon_{CPA}(0) = \upsilon_{CPA}^0 = 0$ @ $t = 0$	(A.2)
$\frac{d\upsilon_{Ions}}{dt} = -P_{Ions} S_{Sph} \Delta M_{Ions}$	$\upsilon_{Ions}(0) = \upsilon_{Ions}^0 = \frac{\left(\upsilon_{Cell}^0 - \upsilon_B\right)}{1 + \frac{\phi}{\widetilde{\upsilon}_{Ions} M^0}}$ @ $t = 0$	(A.3)
$\frac{dS_{Ref}}{dt} = k_S\, S_{Ref} \Delta\sigma$	$S_{Ref}(0) = S_{Ref}^0 = \frac{S_{Sph}^0}{1 + \frac{2\,\sigma_R}{K}}$ @ $t = 0$	(A.4)

Table A2
AEs of the SAR model [20].

Equation	Number
$\upsilon = \upsilon_B + \upsilon_{Ions} + \upsilon_W + \upsilon_{CPA}$	(A.5)
$\Delta P = P^{INT} - P^{EXT} = \frac{2\,h\Delta\sigma}{r}$	(A.6)
$\Delta\sigma = \sigma - \sigma_R$	(A.7)
$\sigma = \frac{K}{2}\left(\frac{S_{Sph}}{S_{Ref}} - 1\right)$	(A.8)
$S_{Sph} = 4\pi\left(\frac{3\,\upsilon}{4\pi}\right)^{\frac{2}{3}}$	(A.9)
$\Delta\Pi = RT\Delta M = RT\left(M^{INT} - M^{EXT}\right)$	(A.10)
$M^{INT} = M^{INT}_{Ions} + M^{INT}_{CPA}$	(A.11)
$M^{INT}_{Ions} = \frac{\phi\ \upsilon_{Ions}}{\tilde{\upsilon}_{Ions}\ \upsilon_W}$	(A.12)
$M^{INT}_{CPA} = \frac{\upsilon_{CPA}}{\tilde{\upsilon}_{CPA}\ \upsilon_W}$	(A.13)
$M^{EXT} = \left(M^{EXT}_{Ions} + M^{EXT}_{Sucrose} + M^{EXT}_{CPA}\right)$	(A.14)
$\Delta M_{CPA} = M^{INT}_{CPA} - M^{EXT}_{CPA}$	(A.15)
$\Delta M_{Ions} = M^{INT}_{Ions} - M^{EXT}_{Ions}$	(A.16)
$P_{Ions} = \begin{cases} 0 & \Delta\sigma \le 0 \\ P_{Ions} & \Delta\sigma > 0 \end{cases}$	(A.17)

Table A3
Parameter values of the SAR model [20].

Parameter	Value	Unit
$E_{a,CPA}$	72570	[J mol^{-1}]
$E_{a,Ions}$	22150	[J mol^{-1}]
$E_{a,W}$	50000	[J mol^{-1}]
h	0.5	[μm]
K	33000	[Pa]
k_S	$3.7\bullet10^{-6}$	[Pa^{-1} s^{-1}]
L_P^{∞}	64.2	[μm Pa^{-1} s^{-1}]
P_{CPA}^{∞}	$1.268\bullet10^{12}$	[μm s^{-1}]
P_{Ions}^{∞}	$4.47\bullet10^{-3}$	[μm L s^{-1} mOsm^{-1}]
R	8.314472	[J mol^{-1} K^{-1}]
σ_R	826	[Pa]
ν_B	0.2	[−]
$\tilde{\upsilon}_{CPA}$	$7.1\bullet10^{-5}$	[m^3 mol^{-1}]
$\tilde{\upsilon}_{Ions}$	$2.7\bullet10^{-5}$	[m^3 mol^{-1}]
ϕ	2	[−]

Nomenclature

k_{CE}	Cytotoxic effect reaction rate constant [s^{-1}]
k_{EL}	Expansion lysis reaction rate constant [s^{-1}]
$E_{a,CE}$	Activation Energy of the Cytotoxic effect [J mol^{-1}]
f_{EL}	Expansion lysis probability density function [Pa^{-1}]
G_{υ}	Cell volume rate variation [μm^3 s^{-1}]
K_W	Shape factor in expansion lysis probability density function [−]
M	Osmolality [mOsm L^{-1}]
n	Cell number density distribution [μm^{-3}]
N	Cell number [-]
P_{Ions}	Ion Permeability [μm L s^{-1} mOsm^{-1}]
R	Universal Gas Constant [J mol^{-1} K^{-1}]
R_V	Viability Ratio [−]
T	Temperature [K]
t	Time [s]
υ	Cell Volume [μm^3]
α	Cytotoxic effect reaction rate parameter [−]
γ	Transition function [Pa^{-1}]
σ	Cell Membrane Tension [Pa]

Superscripts

INT	referred to the intracellular solution
0	referred to the initial time

Subscripts

CPA	referred to the CPA
Break	referred to the expansion lysis breakage limit
Mean	Mean value
NV	Non-Viable Cells
R	referred to the resting condition
TOT	Total Cells
V	Viable Cells

References

[1] Y. Han, X. Li, Y. Zhang, Y. Han, F. Chang, J. Ding, Mesenchymal stem cells for regenerative medicine, Cells 8 (8) (2019), https://doi.org/10.3390/cells8080886. ISSN 2073-4409.

[2] Y. Tang, Y. Zhou, H.-J. Li, Advances in mesenchymal stem cell exosomes: a review, Stem Cell Res. Ther. 12 (1) (2021), https://doi.org/10.1186/s13287-021-02138-7.

[3] G. Traversari, A. Cincotti, Insights into the model of non-perfect osmometer cells for cryopreservation: a parametric sweep analysis, Cryobiology 100 (2021) 193–211, https://doi.org/10.1016/j.cryobiol.2020.11.013.

[4] I. Ullah, R. Subbarao, G. Rho, Human mesenchymal stem cells - current trends and future prospective, Biosci. Rep. 35 (2015), https://doi.org/10.1042/BSR20150025.

[5] H. Jin, Y. Bae, M. Kim, S.-J. Kwon, H. Jeon, S. Choi, S. Kim, Y. Yang, W. Oh, J. Chang, Comparative analysis of human mesenchymal stem cells from bone marrow, adipose tissue, and umbilical cord blood as sources of cell therapy, Int. J. Mol. Sci. 14 (9) (2013) 17986–18001, https://doi.org/10.3390/ijms140917986.

[6] I. Arutyunyan, T. Fatkhudinov, G. Sukhikh, Umbilical cord tissue cryopreservation: a short review, Stem Cell Res. Ther. 9 (1) (2018), https://doi.org/10.1186/s13287-018-0992-0.

[7] S. Fadda, H. Briesen, A. Cincotti, The effect of EIF dynamics on the cryopreservation process of a size distributed cell population, Cryobiology 62 (3) (2011) 218–231, https://doi.org/10.1016/j.cryobiol.2011.03.006.

[8] S. Fadda, A. Cincotti, G. Cao, The effect of cell size distribution during the cooling stage of cryopreservation without CPA, AIChE J. 56 (8) (2010) 2173–2185, https://doi.org/10.1002/aic.12137.

[9] S. Fadda, A. Cincotti, G. Cao, Rationalizing the equilibration and cooling stages of cryopreservation: the effect of cell size distribution, AIChE J. 57 (4) (2011) 1075–1095, https://doi.org/10.1002/aic.12320.

[10] D. Berz, E.M. McCormack, E.S. Winer, G.A. Colvin, P.J. Quesenberry, Cryopreservation of hematopoietic stem cells, Am. J. Hematol. 82 (6) (2007) 463–472, https://doi.org/10.1002/ajh.20707.

[11] P. Mazur, Freezing of living cells: mechanisms and implications, Am. J. Physiol. Cell Physiol. 247 (3) (1984) C125–C142, https://doi.org/10.1152/ajpcell.1984.247.3.C125.

[12] A.A. Gurtovenko, J. Anwar, Modulating the structure and properties of cell membranes: the molecular mechanism of action of dimethyl sulfoxide, J. Phys. Chem. B 111 (35) (2007) 10453–10460, https://doi.org/10.1021/jp073113e.

[13] H. Meryman, Osmotic stress as a mechanism of freezing injury, Cryobiology 8 (5) (1971) 489–500, https://doi.org/10.1016/0011-2240(71)90040-X. ISSN 0011-2240.

[14] K. Muldrew, L. McGann, The osmotic rupture hypothesis of intracellular freezing-injury, Biophys. J. 66 (2) (1994) 532–541, https://doi.org/10.1016/S0006-3495(94)80806-9. ISSN 0006-3495.

[15] J. Wolfe, M. Dowgert, P. Steponkus, Mechanical study of the deformation and rupture of the plasma-membranes of protoplasts during osmotic expansions, J. Membr. Biol. 93 (1) (1986) 63–74, https://doi.org/10.1007/BF01871019. ISSN 0022-2631.

[16] E. Casula, G.P. Asuni, V. Sogos, A. Cincotti, hMSCs from UCB: isolation, characterization and determination of osmotic properties for optimal cryopreservation, Chem. Eng. Trans. 43 (2015) 265–270, https://doi.org/10.3303/CET1543045.

[17] E. Casula, G.P. Asuni, V. Sogos, S. Fadda, F. Delogu, A. Cincotti, Osmotic behaviour of human mesenchymal stem cells: implications for cryopreservation, PLoS One 12 (9) (2017) 1–21, https://doi.org/10.1371/journal.pone.0184180.

[18] F. Kleinhans, Membrane permeability modeling: kedem-katchalsky vs a two-parameter formalism, Cryobiology 37 (4) (1998) 271–289, https://doi.org/10.1006/cryo.1998.2135.

[19] E. Casula, G. Traversari, S. Fadda, O.V. Klymenko, C. Kontoravdi, A. Cincotti, Modelling the osmotic behaviour of human mesenchymal stem cells, Biochem. Eng. J. 151 (2019) 107296, https://doi.org/10.1016/j.bej.2019.107296.

[20] G. Traversari, F. Delogu, S. Aparicio, A. Cincotti, hMSCs in contact with DMSO for cryopreservation: experiments and modelling of osmotic injury and cytotoxic effect, Biotechnol. Bioeng. 119 (10) (2022) 2890–2907, https://doi.org/10.1002/bit.28174.

[21] D.M. Himmelblau, K.B. Bischoff, Process Analysis and Simulation: Deterministic Systems, John Wiley & Sons, New York, 1968, pp. 66–68.

[22] D. Ramkrishna, Population Balances-Theory and Applications to Particulate Systems in Engineering, Academic Press, San Diego, 2000.

[23] J.D. Benson, A.J. Kearsley, A.Z. Higgins, Mathematical optimization of procedures for cryoprotectant equilibration using a toxicity cost function, Cryobiology 64 (3) (2012) 144–151, https://doi.org/10.1016/j.cryobiol.2012.01.001.

[24] A.F. Davidson, C. Glasscock, D.R. McClanahan, J.D. Benson, A.Z. Higgins, Toxicity minimized cryoprotectant addition and removal procedures for adherent endothelial cells, PLoS One 10 (11) (2015) e0142828, https://doi.org/10.1371/journal.pone.0142828.

[25] H.Y. Elmoazzen, A. Poovadan, G.K. Law, J.A.W. Elliott, L.E. McGann, N.M. Jomha, Dimethyl sulfoxide toxicity kinetics in intact articular cartilage, Cell Tissue Bank. 8 (2007) 125–133, https://doi.org/10.1007/s10561-006-9023-y.